Thermal management of electric vehicle battery cells with homogeneous coolant and temperature distribution ⒡

ⓘD Sinan Gocmen, ⓘD Sahin Gungor and ⓘD Erdal Cetkin

COLLECTIONS

Ⓕ   This paper was selected as Featured

🌐   ⬆   🔴
View Online   **Export Citation**   **CrossMark**

ARTICLES YOU MAY BE INTERESTED IN

Thermal management of electric vehicle battery cells with homogeneous coolant and temperature distribution Ⓕ

Sinan Gocmen,[1] Ⓘ Sahin Gungor,[1,2] Ⓘ and Erdal Cetkin[1,a)] Ⓘ

AFFILIATIONS

[1]Department of Mechanical Engineering, Izmir Institute of Technology, Urla, Izmir 35430, Turkey
[2]Department of Mechanical Engineering, Izmir Katip Celebi University, Cigli, Izmir 35620, Turkey

[a)]**Author to whom correspondence should be addressed:** erdalcetkin@gmail.com and erdalcetkin@iyte.edu.tr

ABSTRACT

Electric vehicles play an integral role in eliminating pollution related to transportation, especially if the electricity is generated via renewable sources. However, storing electricity onboard requires many battery cells. If the temperature of the cells is not strictly regulated, their capacity decreases in time, and they may burn or explode due to thermal runaway. Battery thermal management systems emerged for safe operations by keeping the battery cell temperatures under limit values. However, the current solutions do not yield uniform temperature distribution for all the cells in a pack. Here, we document that constant temperature distribution can be achieved with uniform coolant distribution to the channels located between batteries. The design process of the developed battery pack begins with a design used in current packs. Later, how the shape of the distributor channel affects flow uniformity is documented. Then, the design complexity was increased to satisfy the flow uniformity condition, which is essential for temperature uniformity. The design was altered based on a constructal design methodology with an iterative exhaustive search approach. The uncovered constructal design yields a uniform coolant distribution with a maximum of 0.81% flow rate deviation along channels. The developed design is palpable and easy to manufacture relative to the tapered manifold designs. The results also document that the peak temperature difference between the cells decreases from a maximum of 12 K to 0.4 K. Furthermore, homogenous distribution of air is one of the limiting factors of the development of metal–air batteries. This paper also documents how air can be distributed uniformly to metal–air battery cells in a battery pack.

Published under license by AIP Publishing. https://doi.org/10.1063/5.0004453

NOMENCLATURE

c_p	specific heat capacity (J kg^{-1} K^{-1})
k	turbulent kinetic energy (m^2 s^{-2})
$\dot{m}$	mass flow rate (kg s^{-1})
P	pressure (Pa)
$\bar{P}$	average pressure (Pa)
$\dot{Q}$	heat generation rate (W)
T	temperature (K)
$\bar{T}$	average temperature (K)
u	velocity vector (m s^{-1})
u'	fluctuations of velocity in each direction (m s^{-1})
$\bar{u}$	average velocity component in each direction (m s^{-1})
x	component of the coordinate system (m)

Greek letters

ΔT	temperature difference (K)
ε	turbulent kinetic energy dissipation rate (m^2 s^{-3})
μ	viscosity (Pa s)
ρ	density (kg m^{-3})
σ_k	turbulent Prandtl number for k (dimensionless)
σ_ε	turbulent Prandtl number for ε (dimensionless)
σ_{cp}	turbulent Prandtl number based on specific heat at constant pressure (dimensionless)

Subscripts

i	ith component of the vector field

in   value at the inlet section
j jth component of the vector field
out   value at the outlet section
t   turbulent term

INTRODUCTION

Pollution related to fossil fuel usage paves the road for the usage of renewable alternatives in industry and transportation.[1–3] Currently, many automotive, software, and defense companies invest in the development of electric and hybrid vehicles. These vehicles generally come with rechargeable lithium-ion (Li-ion) batteries that have advantages in comparison to competing batteries such as greater energy density, specific power and recyclability, lightweight, lower self-discharge rate, and longer life cycle. Therefore, the literature focuses on the possible advancements of Li-ion battery systems.[4–7] Nonetheless, the heat generated from battery cells during charge and discharge should be transferred from the pack which includes hundreds (or thousands depending on the type) of cells. The lack of cooling decreases the lifetime of battery cells or they may even explode (due to thermal runaway). Hence, battery thermal management systems (BTMS) have emerged with the aim of cooling of cells in battery packs to prevent thermal runaway.[8–10] Pesaran[11,12] also documented that BTMS should be capable of ventilation to exhaust potentially hazardous gases from the pack and cooling to control the temperature of battery cells.

Air-cooled BTMSs are the most preferred single-phase cooling solution due to the ease of integration with other methods and applications. Accordingly, there are numerous numerical and experimental studies on air-cooled BTMSs.[13–20] For instance, Chen et al.[13–16] documented the effect of spacing between the battery cells for several manifold models with air cooling. Park[17] analyzed the cooling performance of five manifold designs without changing the layout or design of the existing battery system. Xu and He[18] performed the numerical analysis of various airflow duct models for cooling with air, and they recommend a double U-type design. Sun and Dixon[19] examined the thermal behavior of Li-ion pouch cells used in hybrid electric vehicles. They showed that a Z-type manifold decreases fluctuation in temperature distribution and performs the best with conductive cooling plates relative to the competing designs. Xie et al.[20] documented numerically the effect of inlet angle and gap between Li-ion battery cells in a pack. They documented that the maximum temperature and temperature difference become minimum when the air inlet and outlet angles are 2.5°. Cetkin[21] documented how the manifold shape should be in order to distribute fluid evenly to channels of a microdevice. Labaek et al.[22] documented the pressure drop and air distribution of two distinct manifold models experimentally for fuel cell applications: U- and Z-type. They showed that the diffuser-type connection enhances flow rate uniformity; however, the variation in flow rate distribution varies between 10 and 20% even for the improved design. Shadid and Chaab[23] numerically documented the thermal performance of various manifold models for packs with cylindrical Li-ion battery cells. They showed that case B is the best design in terms of temperature uniformity where the maximum temperature in the pack can be reduced by 9%. Chen et al.[24] documented the effect of air inlet and outlet port locations on peak temperature and maximum cell temperature difference.

The literature also documents that the theoretical energy density of metal–air batteries is much greater (3–30 times) than the lithium-ion batteries.[25] Yet, oxygen reactions should be enhanced for palpable devices. Hence, researchers focus on the development of materials for metal–air batteries.[26–29] In addition, the amount of supplied oxygen/air to the cathode is of paramount importance. For instance, Park et al.[30] documented the double oxygen supply system to enhance the capacity of a Li-O$_2$ battery. The literature focuses on the supply of oxygen/air at the cell level. However, current battery pack designs do not conform flow uniformity which would create nonuniform battery capacities in a pack of metal–air batteries. Overall, achieving homogeneous distribution of air to the cells in a pack maximizes the performance of metal–air batteries and conforms uniform temperature distribution in a Li-ion battery pack.

Although there are many publications on the thermal management of battery packs, the literature lacks in documenting how battery packs should be designed in order to distribute the coolant/air effectively and control the battery cell temperature strictly. Rather, the literature relies on improvements of manifold designs where random design parameters or port positions are analyzed. Here, we document how all the battery cells can be kept under the desired temperature with the improved battery pack design for advanced electric vehicles by considering a constructal design approach. The developed design is aimed to distribute fluid evenly by achieving the same pressure drop along each flow path between battery cells. The uniform distribution of air to each cell of a pack eliminates the nonuniform capacities of metal–air batteries in packs.

MODEL

Figure 1(a) shows the battery pack of a commercial vehicle (Chevrolet Volt). Figure 1(b) illustrates the numerical solution domain where battery cells and air domains are represented in gray and transparent fashions, respectively. Figure 1(b) also includes the zoomed view of two distinct regions with their mesh elements. There are 15 battery cells that are compatible with the electric vehicle industry, i.e., modules with 6–24 cells are common. In addition, Fig. 1 documents the elemental volume representation of battery cells with spacing between them; the zoomed view of the meshed domains is also included. Coolant enters the Z-type manifold from the top at 10 m/s and 298 K and is distributed to the spacing between battery cells as shown in Fig. 1(b). Then, it is collected and leaves from the collector where the outlet boundary condition is zero gauge pressure. The design in Fig. 1(b) is of the Z-type because the coolant flows along a path looks like Z, the inlet and outlet ports farther from each other and but the flow direction is the same. This manifold shape was selected due to their enhanced flow uniformity in comparison to the U-type designs.[16,19] U-type manifolds have inlet and outlet ports on the same surface but the flow direction is the opposite of the inlet direction. This allows a major portion of the fluid to bypass cooling channels and flow directly from the inlet to the outlet.

Figure 1(c) indicates the boundary conditions for the elemental volume. Please note that conservation of energy is satisfied at
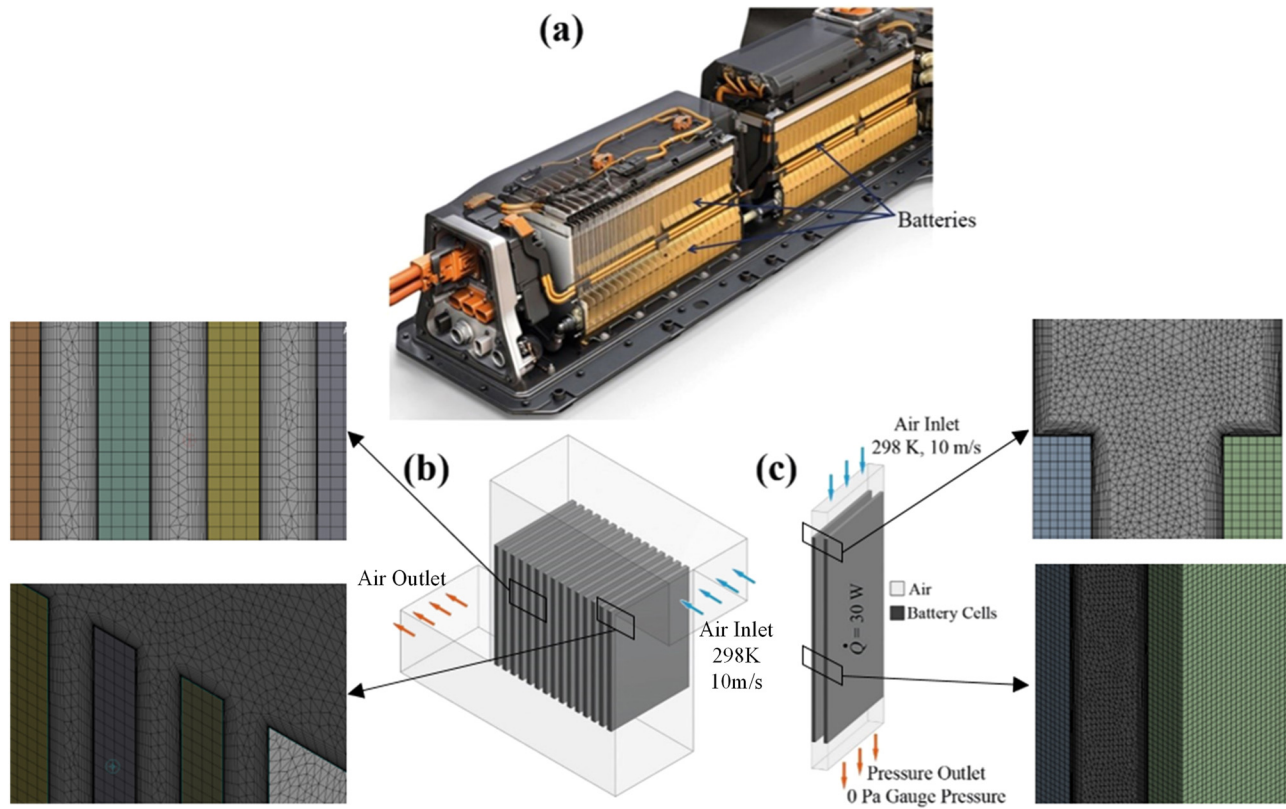
FIG. 1. (a) Battery pack of Chevrolet Volt, (b) Z-type manifold, and (c) elemental volume.

the interfaces of battery cell surfaces and air. In order to document the effect of spacing between cells, first numerical domains (two battery cells and air domain between them) of Fig. 1(c) were simulated. Thus, the simulation time was decreased greatly. Please note that the chief assumption is that the fluid is distributed uniformly (which is also going to be discussed) to each channel to uncover the minimum channel length required for effective cooling.

The fluid flow is assumed as incompressible because the density change in the domain is negligibly small for all cases. In addition, it is assumed to be steady state because the conditions are more challenging than many time-dependent case study conditions which indicate that the uncovered designs will be applicable for many distinct cases. Reynolds number is greater than the critical Reynolds number; therefore, the flow is turbulent. With all these in mind, the conservation of mass, momentum, and energy equations in averaged form become[31,32]

$$\frac{\partial \bar{u}_j}{\partial x_j} = 0,\qquad(1)$$

$$\frac{\partial}{\partial x_j}(\rho \bar{u}_i \bar{u}_j) = -\frac{\partial \bar{P}}{\partial x} + \frac{\partial}{\partial x_j}\left[\mu\left(\frac{\partial \overline{u_i}}{\partial x_j} + \frac{\partial \overline{u_j}}{\partial x_i}\right)\right] - \frac{\partial}{\partial x_j}(\rho \overline{u'_i u'_j}),\qquad(2)$$

$$\frac{\partial}{\partial x_j}(\rho \bar{u}_j \bar{T}) = \frac{\partial}{\partial x_j}\left(\frac{\mu}{\sigma_{cp}}\frac{\partial \bar{T}}{\partial x_j}\right) - \frac{\partial}{\partial x_j}(\rho \overline{u'_j T'}),\qquad(3)$$

where $\bar{u}$, $\bar{v}$, $\bar{w}$, $\bar{P}$, and $\bar{T}$ are the average x-, y-, and z-velocity components, average pressure, and average temperature, respectively. u', v', and w' are the fluctuations of velocity in each direction, μ is the dynamic viscosity, and σ_{cp} is the molecular Prandtl number defined by the specific heat at constant pressure. The k–ε turbulent model was chosen as a viscous turbulent model due to its simplicity and validity in internal flows, that is,

$$\frac{\partial}{\partial x_i}(\rho k \bar{u}_i) = \frac{\partial}{\partial x_j}\left[\left(\mu + \frac{\mu_t}{\sigma_k}\right)\frac{\partial k}{\partial x_j}\right] - \rho \overline{u'_i u'_J}\frac{\partial u_j}{\partial x_i} - \rho\varepsilon,\qquad(4)$$

$$\frac{\partial}{\partial x_i}(\rho \varepsilon \bar{u}_i) = \frac{\partial}{\partial x_j}\left[\left(\mu + \frac{\mu_t}{\sigma_\varepsilon}\right)\frac{\partial \varepsilon}{\partial x_j}\right] + C_1\frac{\varepsilon}{k}\left(-\rho \overline{u'_i u'_J}\frac{\partial u_j}{\partial x_i}\right) - C_2\rho\frac{\varepsilon^2}{k},\qquad(5)$$

$$\mu_t = \rho C_\mu \frac{k^2}{\varepsilon},\qquad(6)$$

where μ_t, ε, k, C_μ, σ_k, and σ_ε are eddy viscosity, eddy dissipation

TABLE I. Mesh independency results for manifold model.

Number of mesh elements	Temperature values (K)			Relative error (%)		
	Outlet	Maximum	Mean	Outlet temperature	Maximum temperature	Mean temperature
14140	305.124	338.574	318.278	…	…	…
44 969	305.108	325.304	313.700	0.0053	3.9193	1.4383
153 470	305.084	324.933	312.741	0.0078	0.1141	0.3058
300 298	305.076	324.444	311.977	0.0028	0.1505	0.2443
352 057	305.075	324.917	311.887	0.0003	0.1459	0.0290
401 282	305.072	325.931	311.898	0.0009	0.3121	0.0036
480 305	305.072	325.877	311.819	0.0001	0.0167	0.0252

rate, turbulence energy term, empirical coefficient, and turbulent Prandtl numbers for k and ε, respectively, which are $C_\mu = 0.09$, $C_1 = 1.44$, $C_2 = 1.92$, $\sigma_k = 1$, and $\sigma_\varepsilon = 1.3$.[33]

The mesh is tetrahedral with inflation on battery cell walls. The mesh size was varied to find out which mesh size yields results free of size effect. A SIMPLE algorithm was used for pressure and velocity coupling. The convergence criterion for iterations is 10^{-6} for all the terms in the simulations. Table I shows the effect of mesh size on the outlet, maximum, and mean temperatures and their relative errors. Mesh size was decreased until the relative error values become $<10^{-3}$. Overall, the mesh with $\sim 4.8 \times 10^5$ elements was chosen because all the relative errors become negligibly small, i.e., $<0.03\%$.

Figure 2 shows that the volumetric flow rate along each channel between two cells for our current approach as well as Park[17] and Chen *et al.*[16] Overall, Fig. 2 shows that the results of the current study are in agreement with the results of Park[17] and Chen *et al.*[16]
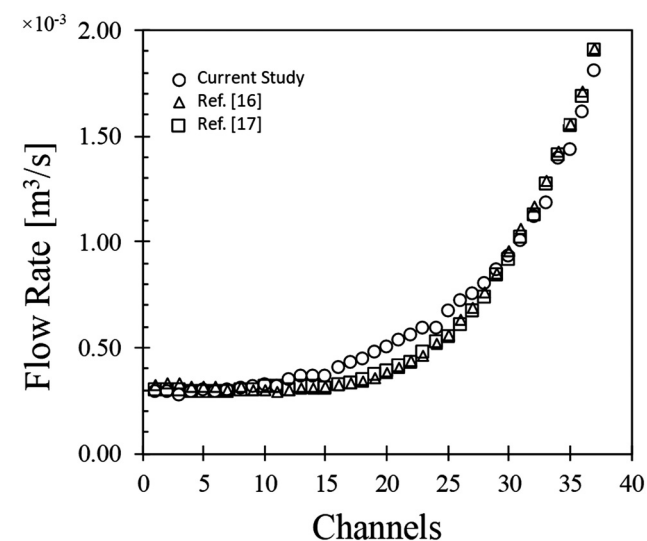
SPACING BETWEEN BATTERY CELLS

The literature shows that spacing between heat-generating domains can be optimized when they are packed into a finite space.[34] Accordingly, first, we survey what should be the optimal spacing between each Li-ion battery cell to achieve effective thermal management with maximum possible energy density in the battery pack. Figure 1(c) shows that air enters an elemental flow volume in the pack with inlet velocity and temperature of 10 m/s and 298 K. Then, it sweeps the surfaces of the battery cells and leaves where the outlet pressure is a zero gage pressure. The heat generated volumetrically in each battery cell with a magnitude of 30 W.[35–38] This volumetric heat generation rate corresponds to the maximum heat generation for 14.6 Ah battery cells under 5C discharge.[35] The change in the air temperature at the outlet can be calculated from

$$\dot{Q} = \dot{m}c_p(T_{out} - T_{in}). \quad (7)$$

Table II documents that the air outlet temperature calculated analytically [Eq. (7)] and numerically are in agreement. It also shows that the current model is valid. In addition, Table II shows that the change in the outlet temperature becomes less than 0.5 K as the spacing increases from 7 to 9 mm. Furthermore, the outlet temperature stays almost the same for 9–13 mm spacing.

FIG. 2. The results of validation study.

TABLE II. The effect of distance between battery cells with air inlet velocity of 10 m/s.

Distance (mm)	Reynolds number	Outlet temperature, Eq. (7) (K)	Outlet temperature (numerical) (K)	Error (%)
3	3557	303.17	303.54	0.1206
5	5855	301.10	301.56	0.1511
7	8098	300.21	300.51	0.0974
8	9198	299.94	300.15	0.0699
9	10 286	299.72	299.79	0.0218
11	12 422	299.41	299.40	0.0036
13	14 508	299.19	299.24	0.0153
16	17 547	298.17	297.95	0.0746

BTMSs should be as compact as possible in order to satisfy the requirements of advanced vehicles, i.e., maximum possible energy density with uniform temperature distribution. The spacing which performs almost as good as the best one with the smallest possible distance is 8 mm. Therefore, the spacing between the battery cells is selected as 8 mm throughout this study.

Consider the base design of Fig. 3(a) with 15 pouch cell batteries and constant diameter distributor and collector channels. The coolant is distributed to the channels between the battery cells to keep their temperature at the desired level. Nonetheless, as Table I shows the fluid is distributed nonuniformly along the channels with constant diameter pack design. Thus, temperature distributions are not expected to be symmetric for each elemental volume, i.e., some battery cells would exceed the acceptable temperature level while others would be a lot colder than the rest. However, the temperature of the cells can be in the same order if the flow rate distribution becomes uniform.

Figure 3(a) shows the pressure distribution for the base design with channel numbers. The figure shows that the pressure gradients between the entrance and exit of each channel vary greatly. This also explains why the flow rate along each channel is distinct. In addition, Fig. 3(b) shows the flow rate for each channel and their deviation from the average flow rate for two- and three-dimensional models. The flow rate becomes 64.9% less and 73.4% more than the average flow rate for the channel with the flow of minimum (channel 1) and maximum (channel 16) with two-dimensional simulations. In addition, Fig. 3(b) shows that the maximum flow rate is five times greater than the minimum flow rate. Overall, Fig. 3 shows that fluid uniformity can be achieved if the pressure gradient for each channel is of the same order. In addition, Fig. 3 shows that the results of two- and three-dimensional models are in good agreement. The validity of the two-dimensional solution approach was uncovered with a three-dimensional model with the geometry of Fig. 1(b). Therefore, here we handle iterative exhaustive search design process with two-dimensional simulations in order to save time. However, verifying whether the flow uniformity is achieved with two-dimensional end design may require three-dimensional solutions to achieve desired flow uniformity. Please note that here exhaustive search design parameters are decided in each solution from the information supplied from the previous iteration. Consequently, the process in here is not based on trying arbitrary parameter changes in the iterative process which accelerates the design process by decreasing the required number of solutions.

Furthermore, in order to uncover the effect of flow rate magnitude on temperature distribution of battery cells, the energy equation was solved with the conservation of mass and momentum equations for minimum, intermediate, and maximum flow rates values from the base design of Fig. 3(b) and Figs. 4(a)–4(c), respectively. Therefore, the accuracy of the two-dimensional and elemental volume approaches can be further validated which are essential due to their small computational cost relative to the three-dimensional battery pack simulations. Comparison of Figs. 4(a) and 4(b) shows that the maximum battery temperature decreases 11.33 K from channel 1 to 9 (with minimum and intermediate flow rates, respectively). Yet, the battery temperature difference between channel 9 and 16 (intermediate and maximum flow rates, respectively) is 2.15 K as shown in Figs. 4(b) and 4(c). These results show that the peak temperature in battery cells is affected greatly from flow rate nonuniformity. The peak temperature difference between distinct cells increases as the flow rate becomes greater or smaller than the average flow rate. Accordingly, Figs. 4(a)–4(c) show that the fluid uniformity is essential in order to keep battery cell temperatures the same in a pack.

In addition, Fig. 4(d) shows the temperature distribution in the pack for the three-dimensional solution domain of Fig. 1(b).
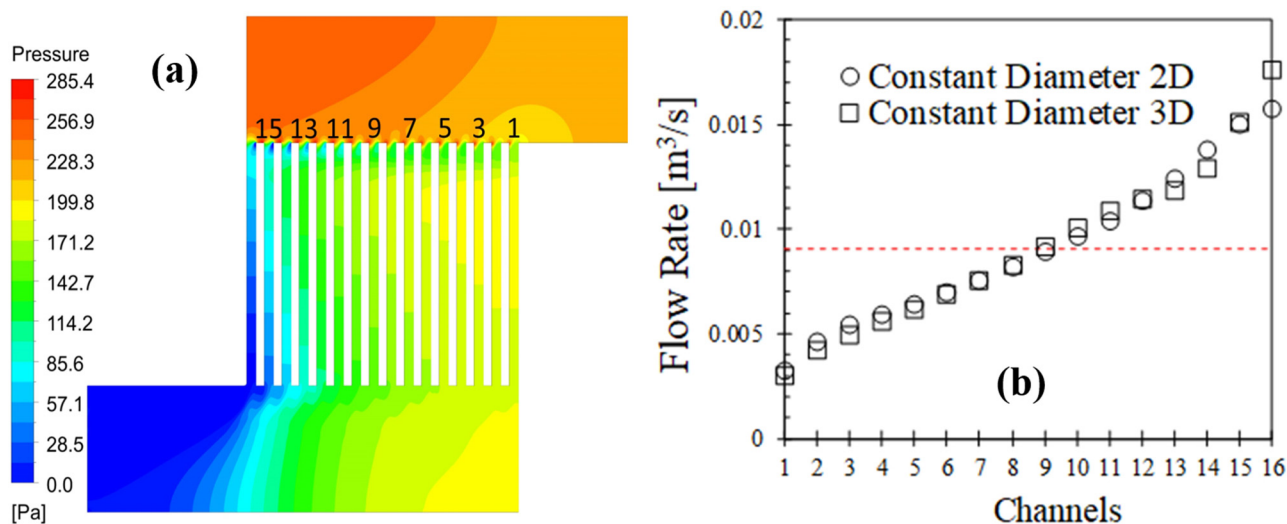

FIG. 3. (a) Pressure distribution of base design and (b) flow rate along each channel.
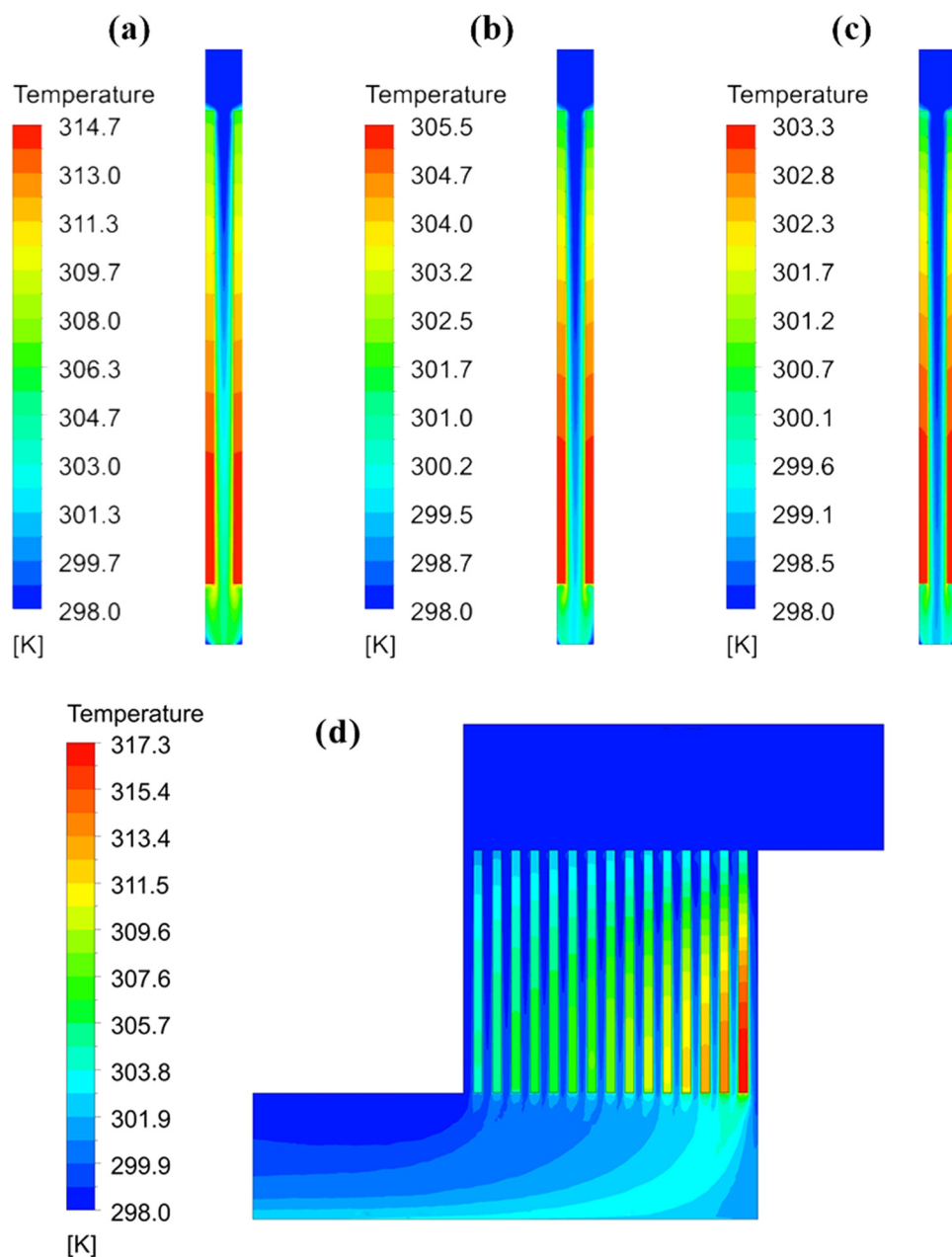
Comparison of Figs. 4(a)–4(c) with Fig. 4(d) shows the accuracy of the two-dimensional solution approach relative to the three-dimensional one in terms of the flow of heat. The temperature difference values are almost the same in the elemental volume approach when compared with the three-dimensional model of the pack. However, the maximum battery cell temperature is greater in Fig. 4(d) relative to Fig. 4(a) as expected because Fig. 3(b) shows that the flow rate along the first channel near the inlet is overestimated in the two-dimensional model. These results show that the optimizing geometric parameters in a two-dimensional model with

the consideration of flow uniformity yields the design of a battery pack with uniform temperature distribution inside of it. Hence, the computational time decreases greatly in the exhaustive search design procedure.

UNIFORM FLOW RATE DISTRIBUTION

In order to have a constant pressure gradient along each channel, the shape of the manifold can be modified. For instance, the diameter of the distributor channel can be contracted as in

Figs. 5(a) and 5(b). Figure 5(a) documents how the pressure distribution varies if the distributor channel is contracted linearly. Figure 5(a) shows that the variation on the pressure gradient along each channel becomes more uniform than Fig. 3 but it is still not as uniform as desired. Especially, the pressure gradient is a lot smaller in the first channel (1–4). Therefore, the contraction is steeped for the first channels, [Fig. 5(b)]. This sudden contraction decreases the variation on pressure but not to the desired level as well. Figure 5(c) shows how the volume flow rates are distributed along each channel for the designs of Figs. 5(a) and 5(b). Figure 5(c) also shows that the sudden contraction design performs slightly better except for the last two channels (channel 15 and 16). This shows that contraction enables flow rate distribution uniformity but

linear or sudden contraction does not satisfy the desired uniformity requirement. Consequently, it can be concluded that the design complexity should be increased in order to achieve a uniform flow rate distribution.

A new and more complex (requires more geometrical parameters) manifold design, tapered design, was developed with the constructal design approach in order to distribute coolant along the channels more uniformly. The distributor channel has a sudden contraction at first, and then it is tapered gradually to enhance flow rate distribution uniformity as implied by the results shown in Fig. 5. Figure 6(a) shows how the pressure distribution is affected from tapering the distributor channel. The pressure gradient (flow resistance) along each channel decreases relative to the previous
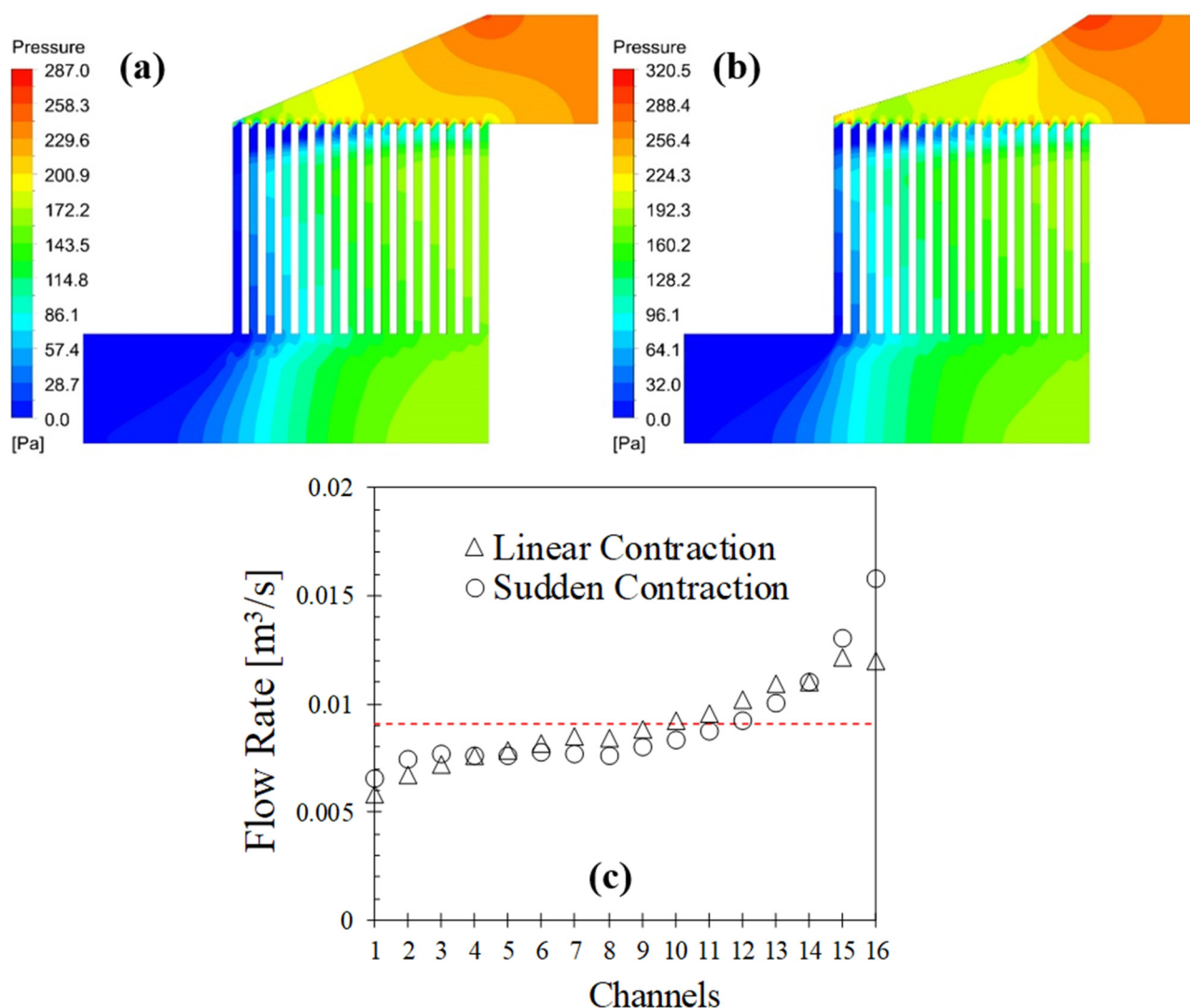

FIG. 5. Pressure distributions of (a) linear contraction and (b) sudden contraction designs and (c) flow rate along each channel.

design shown in Fig. 5(b) (except last two channels, 15 and 16) which has a sudden contraction. However, the overall pressure drop increases in the design shown in Fig. 6(a) relative to the designs shown in Fig. 5 because of the increment in the fluid flow

resistance along the distributor channel. Please note that the distributor is tapered gradually with a linearly contracted channel size along the sections where fluid enters to channel. The flow rate is more uniform in the design shown in Fig. 6(b) relative to the
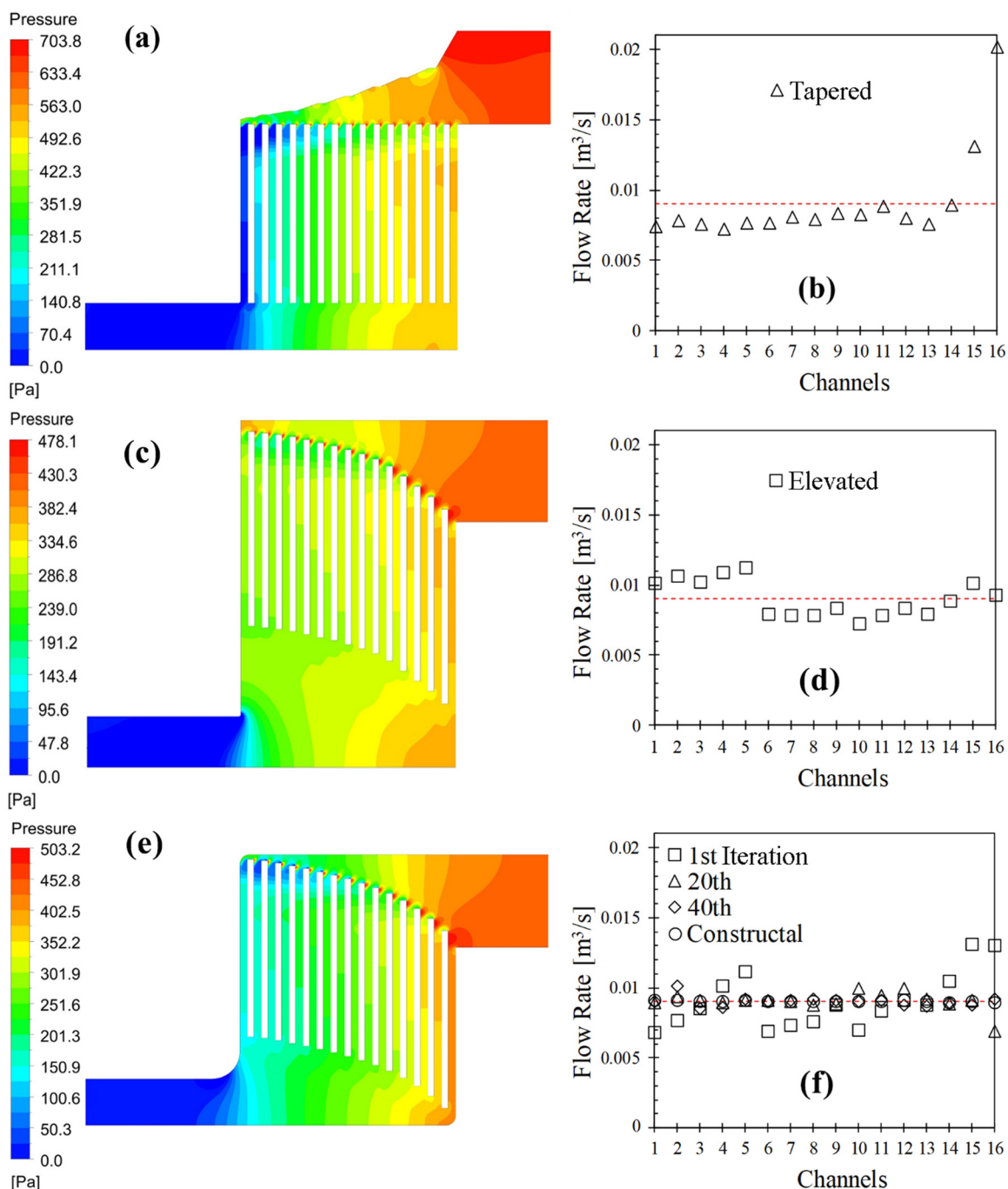

FIG. 6. Pressure distributions and flow rate variations of (a) and (b) tapered design, (c) and (d) elevated design, and (e) and (f) constructal design, respectively.

design shown in Fig. 5(b) except channels 15 and 16. In addition, Fig. 6(b) also documents that the maximum and minimum flow rates are 122.3% more and 20.3% less than the average flow rate (channel 16 and 4, respectively.)

The tapered design shown in Fig. 6(a) was inspired from our previous work of Ref. 21 which was developed for a microdevice. Nonetheless, manufacturing variable cross-section channels are not common due to their complexity. The reason why tapering channel cross section yields better flow uniformity is the pressure gradient along the inlet and outlet of each channel located between the cells can be kept at a constant value. Constant pressure gradient conforms to homogeneous coolant distribution. The pressure gradient between the distributor and collector channels can also be fixed with constant manifold designs as the height of coolant channels embedded into the manifold vary. The manifolds are constant in the cross sections where the vertical position of the battery cells are dispersed exponentially as shown in Fig. 6(c), i.e., the elevated design. The deviation in the flow rate relative to the average flow rate in channels 15 and 16 are reduced to 23.2% and 54%, respectively.
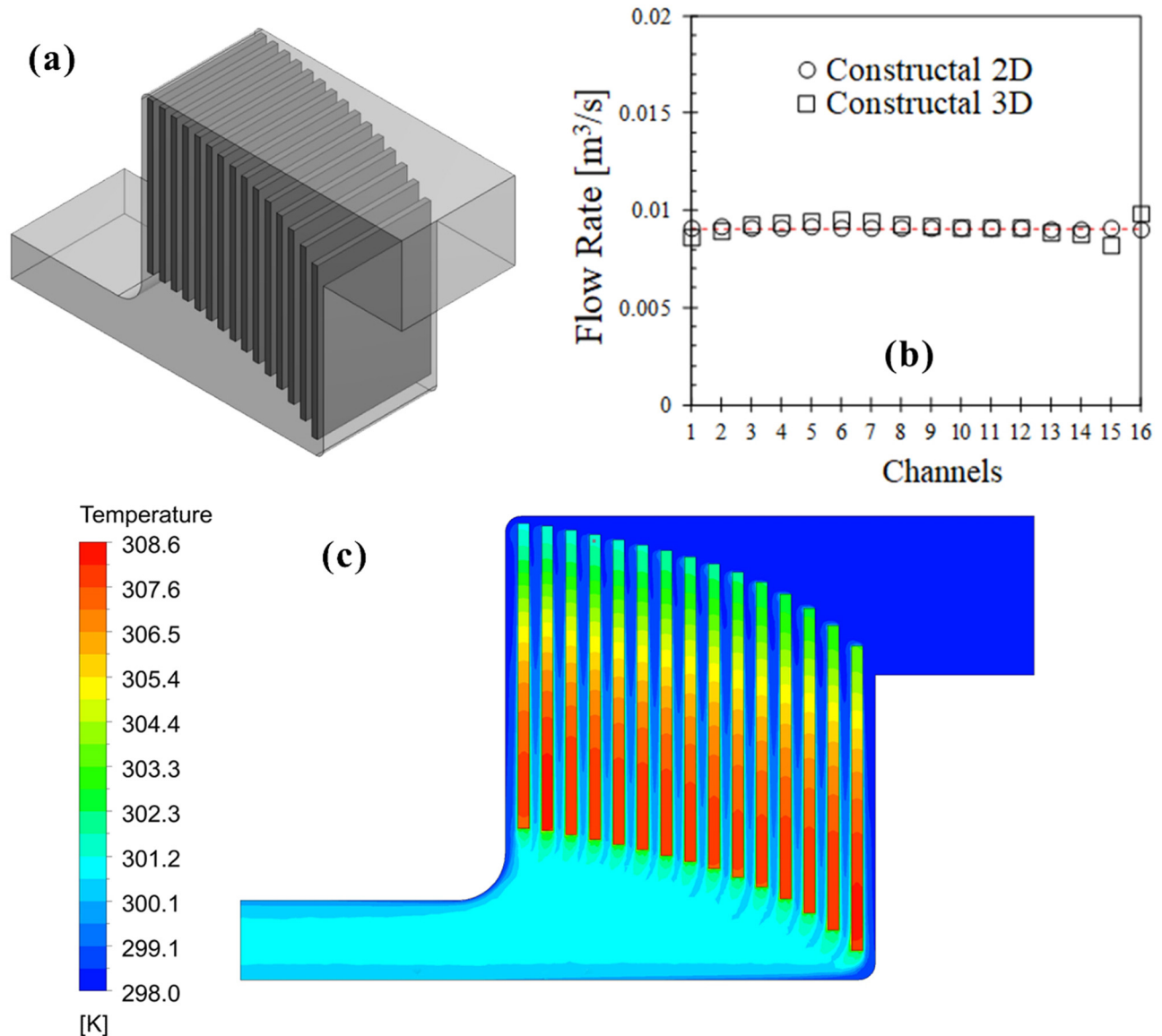

FIG. 7. (a) Three-dimensional model of battery pack with the cell positions of Figs. 6(f) and 6(b) flow rate along each channel for two- and three-dimensional constructal models and (c) temperature distribution of three-dimensional constructal model.

In addition, the comparison of Figs. 6(b) and 6(d) shows the flow rate is distributed more uniformly in the elevated design relative to the tapered one. The comparison of Figs. 6(a) and 6(c) reveals that the pressure drop also decreases as the elevation of battery cells is varied rather than altering the design of distributors. However, the maximum and minimum flow rates are 23.6% more and 8% less than the average flow rate of channels 8 and 5, respectively, which are more than the desired level. In addition, Fig. 6(c) shows that the collector channel becomes very thick near the exit. This fluid domain is excessive, and it increases the pack volume without any purpose. Therefore, the elevated design can be modified by removing the excessive volume of the collector channel. This causes the energy density of the battery pack to enhance greatly, which is essential as the space reserved for the pack is limited.

Next, consider the constructal design with the excess fluid domain near the exit of the manifold is subtracted as shown in Fig. 6(e). In addition, the sharp corners near the inlet and outlet were rounded to get rid of sudden pressure drops. The vertical positions of batteries were optimized iteratively where the stop criterion was maximum 1% fluctuation in flow rate relative to the average value. In order to achieve this criterion, the design was iteratively altered approximately 60 times. Battery positions in the initial design are the same as that shown in Fig. 6(c), 1st design. Yet, Figs. 6(d) and 6(f) show that flow rate distribution becomes worse as the excessive volume near the outlet port is subtracted. It is expected as fluid flow along each channel is governed by the pressure difference between the inlet and outlet of each channel. Varying geometrical parameters at the collector channel affect the pressure distribution along it and, thus, the flow rate uniformity. Figure 6(f) shows how flow rates along each channel evolve as the design is altered via iterative exhaustive search method. Figure 6(f) documents flow rate distributions for the 1st, 20th, 40th, and last iterations, i.e., the constructal design. Moreover, the flow rates between the channels are almost the same; the maximum flow rate deviation from the average flow rate is 0.81% (channel 5) as shown

in Fig. 6(f). Figure 6(e) also shows the pressure distribution for the constructal design. The pressure distribution along the distributor and collector channels varies greatly. Nonetheless, the pressure gradient along the cooling channels does not vary as much as in tapered and elevated designs. Note that the required pressure increased approximately 200 Pa in the constructal design of Fig. 6(e) relative to the design of Fig. 3(a). The reason for this increment is due to the fluid is forced to flow uniformly along each channel in Fig. 6(e), there is no bypass channel as in the design of Fig. 3(a) where most of the fluid was flowing in several channels due to relatively less flow resistance in comparison to the other channels. The designs in Fig. 6 indicate that flow uniformity requires increment in the pressure drop relative to the base design of Fig. 3.

HOMOGENEOUS TEMPERATURE DISTRIBUTION

The results of Figs. 3 and 4 documented that the two-dimensional solution approach is useful to uncover flow rate uniformity but it lacks in documenting temperature distribution accurately. Thus, the three-dimensional model of a battery pack with the cell positions of constructal design, Fig. 7(a) and 8, was simulated. The three-dimensional simulation confirms that the flow rate distribution calculated with two-dimensional simulations is valid, i.e., the maximum variation in the flow rate is 13.28% for the last two channels and the maximum is 4.67% for the remaining channels [Fig. 7(b)]. Figure 7 also documents that the maximum temperature difference on a single battery is 7 K (it is 5.5 K for the majority of battery cells). These values stay in an acceptable operating temperature range. The comparison of Figs. 4 and 7 shows that cooling the cells in a battery pack can be achieved with the methodology of this study, i.e., locating the battery cells such that the pressure drop along each path line is the same to conform uniform coolant distribution. The approach yields the same temperature distribution for each cell in a pack. So, the temperature in a pack can be regulated strictly with this approach.
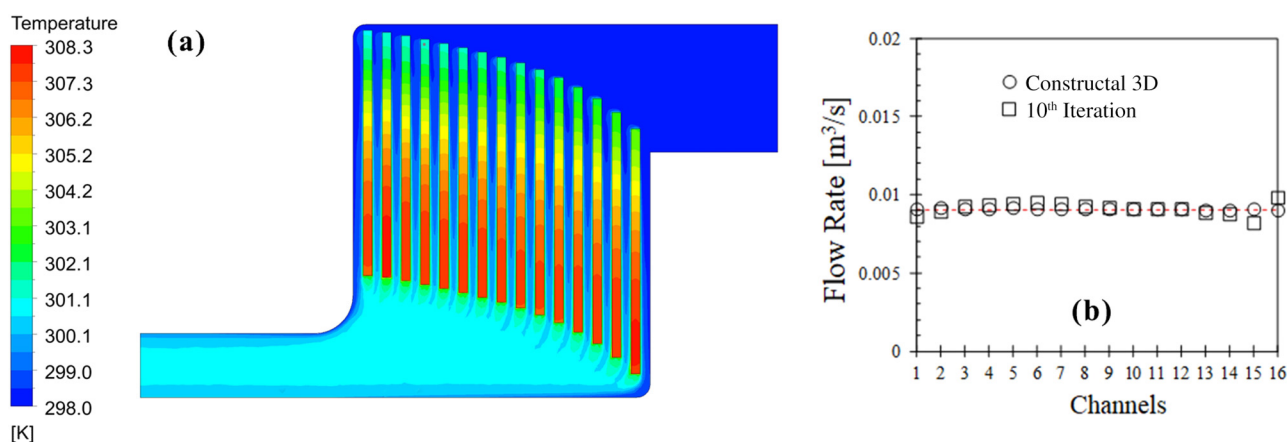

FIG. 8. (a) Temperature distribution of 10th iteration and (b) flow rate in each channel.

However, Fig. 7 shows that there is a mismatch between the two- and three-dimensional solution methods as expected due to the results shown in Fig. 4. Even though it is relatively small, if this mismatch is eliminated, temperature distribution can be more uniform along each battery cell. Therefore, the design shown in Fig. 7 is further improved with iterative exhaustive search by using three-dimensional models. The tenth iteration yields the design with the desired flow rate uniformity as the initial design almost satisfied flow uniformity, as can be seen in Fig. 8. The maximum temperature difference between the peak temperatures of battery cells become less than 0.5 K and the maximum temperature difference in a single battery vary between 6 and 6.5 K. Overall, processing cost has decreased greatly by uncovering the battery locations corresponding to flow uniformity first with two-dimensional simulations and then using it as the initial design for three-dimensional exhaustive search procedure.

According to the results, the constructal design performs much better than all other designs. Overall, this design can be defined as the best design in terms of flow rate distribution uniformity, decreased temperature difference (along batteries and between them) and compactness compared to other competing designs.

CONCLUSION

In this paper, a new battery pack manifold design satisfying the cooling requirements was uncovered with enhanced compactness. In order to eliminate capacity loss and thermal runaway in battery cells, thermal management plays an integral role. Temperature difference in a battery cell should not be more than 6 K to minimize aging as the literature shows. However, the temperature difference between the batteries is also essential and should be avoided as it affects the resistivity of cells directly and yield nonuniform charging/discharging characteristics. The results document that temperature difference between and along battery cells can be minimized if the coolant is distributed uniformly along the channels located between the battery cells. First, the flow rate distribution of a base design is documented. The results show that the maximum temperature difference in a battery cell becomes 16.7 K as it would be 6 K if the coolant was distributed uniformly. Then, the effect of linear and sudden contractions on the distributor channel is documented. The results show that the channel cross section should be tapered with increased complexity. In order to satisfy this, the tapered design was introduced and enhancement in the flow rate distribution is observed. Achieving a uniform flow rate by tapering the channel cross section requires complex channel geometry, which is difficult to manufacture. Next, the collector and distributor cross sections were kept constant and the vertical positions of the battery cells were varied exponentially in elevated design. However, the elevated design includes an excessive flow domain without any purpose and sharp corners. Removing excess volume and rounding sharp corners yielded constructal design. Flow rate uniformity with less than 1% fluctuation is achieved with the constructal design. The flow uniformity of air supplied to each cell is also essential for the applicability of metal–air batteries in battery packs. Therefore, the results of this paper can accelerate the usage of metal–air batteries in battery packs.

In addition, the results document that the two- and three-dimensional models are accurate but there is a mismatch between them, specifically in temperature distribution. Consequently, the two-dimensional constructal design was used as the initial design for the three-dimensional optimization procedure. The results show that the temperature difference between the battery cells in a pack becomes almost the same (<1 K difference). Hence, strict temperature control of battery cells with the approach of this paper can be achieved. Overall, this paper documents a compact BTMS design with uniform coolant distribution to eliminate thermal runaway and capacity loss in battery cells.

DATA AVAILABILITY

The data that support the findings of this study are available from the corresponding author upon reasonable request.

REFERENCES

[1]H. Jouhara, N. Khordehgah, N. Sereya, S. Almahmoud, S. P. Lester, D. Machen, and L. Wrobel, Energy **170**, 849 (2019).
[2]A. Foley and A. G. Olabi, Renew. Sustain. Energy Rev. **68**, 1112 (2017).
[3]H. Jouhara and A. G. Olabi, Energy **160**, 1 (2018).
[4]X. Liu, Z. Chen, C. Zhang, and J. Wu, Appl. Energy **123**, 263 (2014).
[5]H. He, R. Xiong, and H. Guo, Appl. Energy **89**, 413 (2012).
[6]F. Sun, R. Xiong, H. He, W. Li, and J. E. E. Aussems, Appl. Energy **96**, 378 (2012).
[7]Y. Xing, W. He, M. Pecht, and K. L. Tsui, Appl. Energy **113**, 106 (2014).
[8]N. Xue, W. Du, T. A. Greszler, W. Shyy, and J. R. R. A. Martins, Appl. Energy **115**, 591 (2014).
[9]J. Kim, J. Oh, and H. Lee, Appl. Therm. Eng. **149**, 192 (2019).
[10]G. Xia, L. Cao, and G. Bi, J. Power Sources **367**, 90 (2017).
[11]A. A. Pesaran, Battery Man **43**, 34 (2001).
[12]A. A. Pesaran, J. Power Sources **110**, 377 (2002).
[13]K. Chen, Z. Li, Y. Chen, S. Long, J. Hou, M. Song, and S. Wang, Energies **10**, 1677 (2017).
[14]K. Chen, S. Wang, M. Song, and L. Chen, Int. J. Heat Mass Transfer **111**, 943 (2017).
[15]K. Chen, Y. Chen, Z. Li, F. Yuan, and S. Wang, Int. J. Heat Mass Transfer **127**, 393 (2018).
[16]K. Chen, S. Wang, M. Song, and L. Chen, Appl. Therm. Eng. **123**, 177 (2017).
[17]H. Park, J. Power Sources **239**, 30 (2013).
[18]X. M. Xu and R. He, J. Power Sources **240**, 33 (2013).
[19]H. Sun and R. Dixon, J. Power Sources **272**, 404 (2014).
[20]J. Xie, Z. Ge, M. Zang, and S. Wang, Appl. Therm. Eng. **126**, 583 (2017).
[21]E. Cetkin, J. Heat Transfer **139**, 082401 (2017).
[22]J. Labaek, M. Bang, and S. K. Kaer, J. Fuel Cell Sci. Technol. **7**, 61011 (2010).
[23]S. Shadid and M. A. Chaab, Therm. Sci. Eng. Progress **5**, 651 (2018).
[24]K. Chen, W. Wu, F. Yuan, L. Chen, and S. Wang, Energy **167**, 781 (2019).
[25]Y. Li and J. Lu, ACS Energy Lett. **2**, 1370 (2017).
[26]H. J. Yan, B. Xu, S. Q. Shi, and C. Y. Ouyang, J. Appl. Phys. **112**, 104316 (2012).
[27]S. Zhou, N. Liu, Z. Wang, and J. Zhao, ACS Appl. Mater Interfaces **9**, 22578 (2017).
[28]Y. Huang, D. Wu, D. Cao, and D. Cheng, Int. J. Hydrogen Energy **43**, 8611 (2018).

[29]Z. Liu, J. Zhao, Y. Cai, and B. Xu, AIP Conf. Proc. **1794**, 040006 (2017).

[30]S. H. Park, Y. J. Cheon, Y. J. Lee, K. H. Shin, Y. Y. Hwang, Y. S. Jeong, and Y. J. Lee, ACS Appl. Mater. Interfaces **11**, 30872 (2019).

[31]A. Bejan, *Convection Heat Transfer* (Wiley, 2013).

[32]R. W. Fox, A. T. McDonald, P. J. Pritchard, and J. W. Mitchell, *Fluid Mechanics* (Wiley,2016).

[33]ANSYS Fluent Theory Guide 18.2.

[34]A. Bejan and S. Lorente, *Design with Constructal Theory* (John Wiley & Sons, Inc., 2008).

[35]Y. Xie, S. Shi, J. Tang, H. Wu, and J. Yu, Int. J. Heat Mass Transfer **122**, 884 (2018).

[36]S. J. Bazinski and X. Wang, J. Power Sources **305**, 97 (2016).

[37]C. Lin, S. Xu, and J. Liu, Int. J. Hydrogen Energy **43**, 8375 (2018).

[38]L. Sheng, L. Su, H. Zhang, Y. Fang, H. Xu, and W. Ye, Energy Convers. Manage. **180**, 724 (2019).